World Academy of Science, Engineering and Technology
International Journal of Civil and Architectural Engineering
Vol:18, No:9, 2024

Numerical Simulation and Analysis of Axially Restrained Steel Cellular Beams in Fire

Asal Pournaghshband

Open Science Index, Civil and Architectural Engineering Vol:18, No:9, 2024 publications.waset.org/10013796.pdf

***Abstract*—**This paper presents the development of a finite element model to study the large deflection behaviour of restrained stainless steel cellular beams at elevated temperature. Cellular beams are widely used for efficient utilization of raw materials to facilitate long spans with faster construction resulting sustainable design solution that can enhance the performance and merit of any construction project. However, their load carrying capacity is less than the equivalent beams without opening due to developing shear-moment interaction at the openings. In structural frames due to elements continuity, such beams are restrained by their adjoining members which has a substantial effect on beams behaviour in fire. Stainless steel has also become integral part of the build environment due to its excellent corrosion resistance, whole life-cycle costs, and sustainability. This paper reports the numerical investigations into the effect of structural continuity on the thermo-mechanical performance of restrained steel beams with circle and elongated circle shapes of web opening in fire. The numerical model is firstly validated using existing numerical results from the literature, and then employed to perform a parametric study. Parametric studies to explore the influence of variation in i) axial restraint stiffness, ii) steel grades, iii) shape and size of web openings, and iv) load level were described. Hence, the structural continuity is evaluated through the application of different levels of axial restraints on the response of carbon steel and stainless steel cellular beam in fire. The transit temperature for stainless steel cellular beam is shown to be less affected by the level of axial stiffness than the equivalent carbon steel cellular beam. Overall, it was established that whereas stainless steel cellular beams show similar stages of behaviour of carbon steel cellular beams in fire, they are capable of withstanding higher temperatures prior to the onset of catenary action in large deflection, despite the higher thermal expansion of stainless steel material.

***Keywords*—**Axial restraint, catenary action, cellular beam, fire, numerical modelling, stainless steel, transit temperature.

I. Introduction

THE use of cellular beams in steel construction has become widespread due to their remarkable mechanical advantages, aesthetic appeal, and efficient accommodation of conduits and building services [1]. Although the reduction of beam weight and cost effectiveness of cellular beam attracted engineers for its adaption in construction projects, the complication of the failure modes of cellular beam became an obstruction. The web openings in cellular beams may trigger unconventional stress distribution within the web which combining with high shear forces acting on the beam yields to an additional local Vierendeel bending across the opening. Unlike solid beams, where failure is predominantly due to flexural yielding, cellular beams exhibit different failure modes, including web-post buckling, tee-section shear, the Vierendeel mechanism, and rupture of the web-post weld [2]-[5]. The increase in the number and the size of web openings also showed to have negative effect on ultimate load capacity and shear resistance of cross section [6]. Furthermore, the steel material properties degraded by increasing temperature. The steel Young's modulus drops drastically by increasing temperature which results in rapid reduction of buckling capacity of cellular beam specifically at the web-post. The widespread use of cellular beams in steelwork projects considering complex failure modes has promoted several investigations into structural performance of cellular beam both at ambient and elevated temperature. The web-post buckling was reported as the critical failure mode of cellular beam with narrow web-posts between closely spaced openings at high temperature [7]. The requirements of coating cellular beams with intumescent fire protection raise remarkable disadvantages on the construction and maintenance cost, and construction period. To eliminate this requirement, an alternative material such as stainless steel can be utilized. Although the behaviour of cold-formed steel cellular beam was studied by many researchers [8]-[10], the performance of stainless steel cellular beam was given little consideration. Stainless steel offers greater retention of strength and stiffness at elevated temperature adding to its significant feature of corrosion resistance attributing to its chromium content [11]. Through investigating beam behaviour with web opening, it was shown that circular openings perform better among all other types of openings. with maximum depth of 75% of the section depth [12]. Furthermore, Rodrigues et al. [13] have demonstrated that beams with circular web openings can bear higher ultimate loads compared to beams featuring other shapes of web openings and it was recommended to use the longitudinal stiffeners welded to horizontal edge of web opening once opening height becomes more than half of beams height. Liu and Chung [14] demonstrated that the steel beam with different shape of web opening develop common failure modes and yield patterns stressing that shape of web opening does not affect steel beam behaviour under a wide range of applied moments and shear forces.

In real building scenarios, steel beams are restrained owing to the presence of surrounding structures. Since rotational restraint has a minimal impact on the beams' response in fire conditions [15], only axial restraint is considered at the beam ends. The stainless-steel structural members have been studied as an isolated elements when subjected to the elevated temperature in current design standards. This methodology ignores the continuities and interaction between individual

Asal Pournaghshband is with University of Hertfordshire, UK (e-mail: a.pournaghshband@herts.ac.uk).

members. However, Nadjai et al. [16] presented the improved structural performance for each individual member in the frame in fire which indicated the conservative approach of standard fire test by disregarding the interaction between members, shown in Fig. 1.

Fig. 1 Fire tests on long cellular beam as isolated and integrated beam in frame structure [16]

It was also established that increase in load ratio for all steel grades results in decrease of fire resistance of the beams with better performance for stainless steel comparing to carbon steel in terms of survival time and deflection [17]. The thermal stress in addition to the degradation of material strength and stiffness at high temperatures generates large deflection that enables evolution of catenary action [18]. Allam et al. [19] investigated the effect of catenary action on heated steel beam by preventing run-away deflection through the experimental and numerical analysis. It was observed that the profile for the large deflection depends on the level of applied load and the stiffness of the surrounding structures affecting the level of axial restraints for the beam. Therefore, design implications for beam with large deflection includes beam's resistance in catenary action [20]. Followed by transmitting catenary action force to the connections and the adjoining structures, it is essential for the beam to survive temperature higher than its limiting temperature and the catenary action force to be sustained by the connections [21]. Therefore, it is crucial to meticulously design cellular steel beams, giving careful consideration to factors such as web-post width, opening size, and material properties. This design process should also account for the effects of catenary action and tensile axial forces originating from adjoining structures.

This study highlights the effect of axial horizontal restraints due to structural continuity on the behaviour of stainless steel cellular beam in catenary action between transit and failure temperature. The main objective of this paper is to present the numerical representation of stainless steel beam survival in fire with different axial restraints via catenary action during large deflection in cellular beams. This study reported the numerical modelling of restrained cellular beam at fire and validation of the model using previous numerical results in the literature. The validated models then were employed to perform parametric analysis with the key parameters involving in the development of catenary action of cellular steel beam such as shape and size of web openings, grades of steel and level of axial restraints. The results of parametric study then were analysed focusing on the large deflection of stainless steel beam with different level of axial restraints.

II. Numerical Modeling

The non-linear finite element analysis package ABAQUS, version 2023 [22] was used to simulate the structural behaviour of cellular steel beams at elevated temperature with different elastic axial behaviour at the ends. Following the validation of numerical model results against existing studies [23], [24] on axially restrained cellular carbon steel beams, this paper proceeds to present the findings of a numerical parametric study conducted on cellular stainless-steel beams. Therefore, the development of the finite element (FE) models, the results from validating existing models in literature, and the successive parametric studies are described.

A. Numerical Results from the Literature

This study conducted a validation of numerical models for axially restrained carbon steel cellular beams under large deflection, exhibiting catenary action at elevated temperatures. The models were validated against prior numerical analyses by Yin and Wang [23] and Najafi [24], focusing on similar beam configurations. The specimens were axially restrained UB457x152x60 of grade S275 carbon steel with nominal length of 8 meters and rectangular web openings. The three examined web opening arrangements were: beams without openings (NOW), beams with a single mid-span opening (SWO), and beams with multiple openings (MWO) located at mid-height. Fig. 2 illustrates these geometric configurations. For the SWO category, three different opening sizes (SWO 1, SWO 2, SWO 3) were explored, drawing from configurations used in the referenced studies. Interestingly, beams with multiple openings exhibited similar behaviour to those without openings, attributable to the size and placement of these openings [23], [24]. The carbon steel beam was subjected to a uniformly distributed load of 35 kN/m (load ratio of 0.7 based on the solid section capacity). The beam was rotationally free with and without full axial restraint. All beams were modelled under uniform temperature distribution following temperature curve from ISO834 [25] and they were assumed to be laterally restrained at every 1000 mm of beam length to prevent lateral-torsional buckling.

Open Science Index, Civil and Architectural Engineering Vol:18, No:9, 2024 publications.waset.org/10013796.pdf

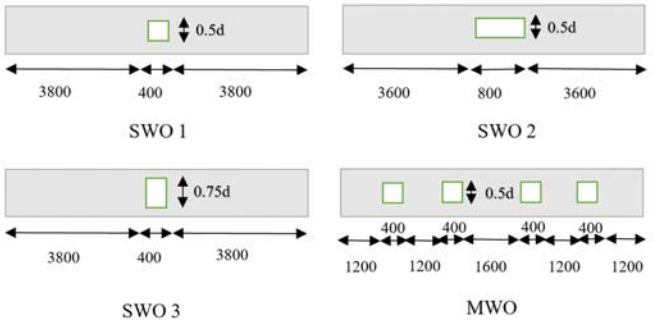

Fig. 2 Geometric arrangement of the simulated beams of Yin and Wang [23] where the dimensions are in mm

B. Description of the FE Models

The temperature-time distribution in the structural members was determined throughout a heat transfer analysis. The heat transfer analysis consisted of transferring heat from fire according to ISO 834 [25] curve to the unprotected beams using a coupled heat transfer mechanism of convection and radiation. In the numerical modelling, radiation was modelled as surface radiation (*SRADIATE) with emissivity coefficient of 0.7 and convection was modelled as a film condition (*SFILM) with convective heat transfer coefficient of 25 W/m²K given in EN 1993-1-2 [25]. The thermal material properties such as thermal conductivity, specific heat and coefficient of thermal expansion were obtained for carbon steel according to EN 1993-1-2 [25] and applied over the full span of the beam. Heat transfer at the flange edges and at the edges of the holes were modelled as concentrated radiation (*CRADIATE) and film condition (*CFILM) with a nodal influence area which was considered as the thickness of the web or flange by the element size. The buckling mode shapes as imperfections were obtained using a linear elastic buckling analysis. Finally, the geometrically and materially non-linear stress analysis was carried out based on the temperature field from the thermal analysis and imperfections from the linear elastic buckling analysis. The structural model of the rotationally free beam with and without full axial restraint was shown in Fig. 3.

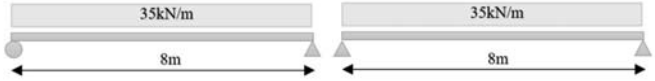

Fig. 3 Structural model of the beam for validation

The beam was modelled with shell elements DS4. The stress-strain at elevated temperature for carbon steel S275 was then obtained using reduction factors set out in EN 1993-1-2 [25]. The true stress σ_{true} and log plastic strain ε_{ln}^{pl}, which were derived from the engineering stress-strain responses, as defined in (1) and (2), respectively, where σ_{nom} is the engineering stress, ε_{nom} is the engineering strain and E is the Young's modulus were incorporated into the numerical models.

$$\sigma_{true} = \sigma_{nom}\left(1+\varepsilon_{nom}\right) \tag{1}$$

$$\varepsilon_{\ln}^{pl} = \ln\left(1+\varepsilon_{nom}\right) - \frac{\sigma_{true}}{E} \tag{2}$$

Imperfections in the form of the lowest global and local buckling modes, obtained from a linear eigenvalue buckling analysis, were assigned to the numerical models. The global imperfection amplitude was set to L/1000, where L is the beam length. The local imperfection as well as residual stresses were ignored based on the assumptions in the previous numerical studies. To simulate the boundary conditions of the experimental set up, the beam end cross-sections were first connected to concentric reference points defined at each beam end through *Rigid Body coupling so that the degrees of freedom of all nodes at beam end cross-section were constrained to the degrees of freedom of their corresponding reference point. The boundary conditions were then assigned to these reference point, RP-1 and RP-2 shown in Fig. 4, where all degrees of freedom were restrained apart from the rotation about the cross-section major axis (UR1 = FREE) at both ends.

Fig. 4 Definition of boundary conditions for the stress analysis model

The geometrically and materially nonlinear stress analysis was carried out in two steps, where in Step 1, the uniformly distributed load was applied to the top surface of the upper flange at room temperature and maintained constant throughout Step 2, where the temperature was increased following the time-temperature relationships stored from the nonlinear thermal analysis model. The general static solver in ABAQUS was used for both Step 1 and Step 2.

Open Science Index, Civil and Architectural Engineering Vol:18, No:9, 2024 publications.waset.org/10013796.pdf

C. Validation Results

The sequentially coupled thermal-stress analysis models were validated against numerical results from literature in this section. Fig. 5 shows the comparison of the failure modes for SWO 2 beam. The failure mode for SWO 2 using ABAQUS showed a very good resemblance with the failure mode of this beam evaluated by Najafi in 2014 [24]. The local buckling of the corners of web opening at the tee-section placed at the top of web openings "top tee section" is captured accurately herein.

Figs. 6-10 compare the FE simulation results for temperature-deflection and temperature-axial reaction of all types of beams assessed in the literature. The unavoidable discrepancies that exist between the previous numerical studies and FE results are due to the lack of information of material properties and simulated temperature distributions. It is concluded that the FE models in this study are able to produce accurate and consistent predictions of the numerical specimen's response given in the literature. Hence, the FE models are suitable for performing parametric studies for restrained cellular beams.

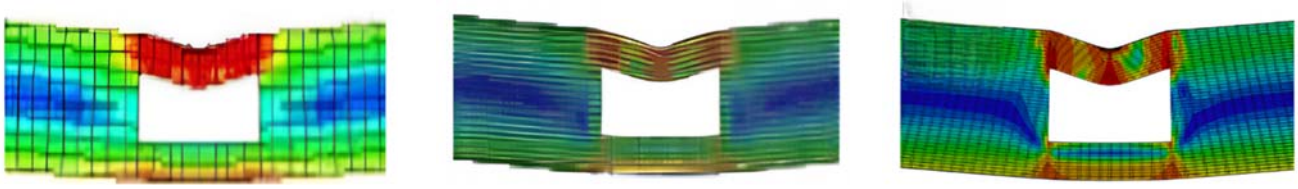

Yin and Wang (2006) [23] Najafi (2014) [24] Author

Fig. 5 Comparison of failure modes at the opening between the simulation results of the author with those of Yin and Wang (2006) [23] and Najafi (2014) [24] for SWO 2

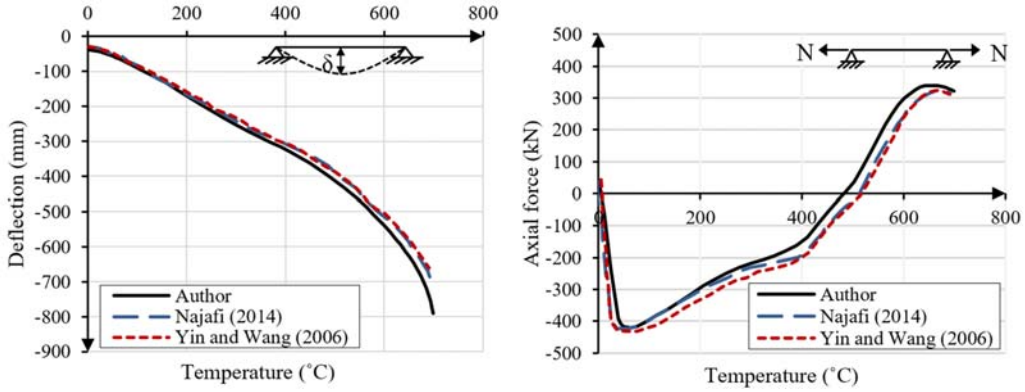

Fig. 6 Comparison of deflection-temperature (LHS) and axial force-temperature responses (RHS) from the simulation results of the author with those of Yin and Wang (2006) [23] and Najafi (2014) [24] for MWO

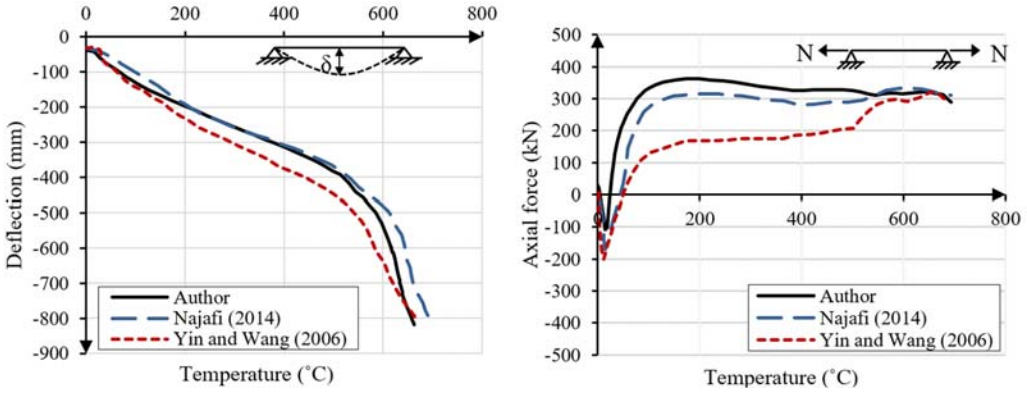

Fig. 7 Comparison of deflection-temperature (LHS) and axial force-temperature responses (RHS) from the simulation results of the author with those of Yin and Wang (2006) [23] and Najafi (2014) [24] for SWO 3

Open Science Index, Civil and Architectural Engineering Vol:18, No:9, 2024 publications.waset.org/10013796.pdf

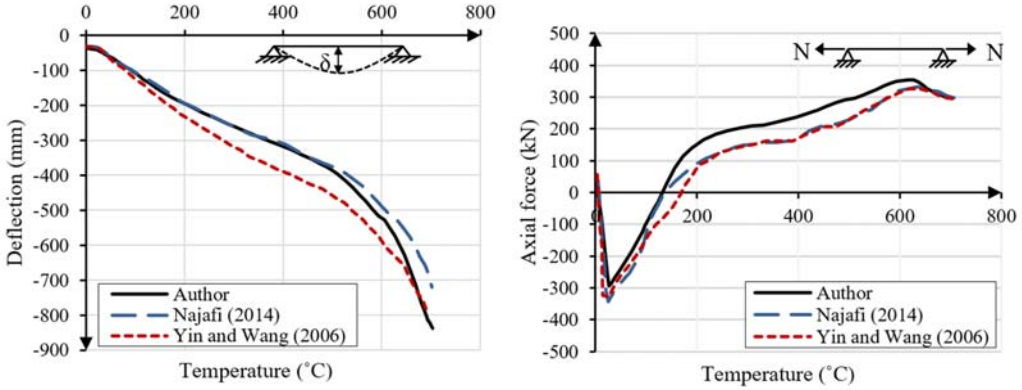

Fig. 8 Comparison of deflection-temperature (LHS) and axial force-temperature responses (RHS) from the simulation results of the author with those of Yin and Wang (2006) [23] and Najafi (2014) [24] for SWO2

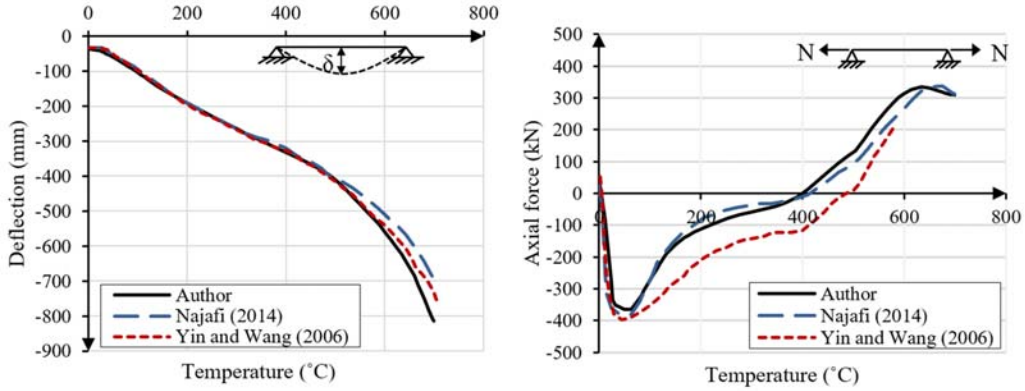

Fig. 9 Comparison of deflection-temperature (LHS) and axial force-temperature responses (RHS) from the simulation results of the author with those of Yin and Wang (2006) [23] and Najafi (2014) [24] for SWO1

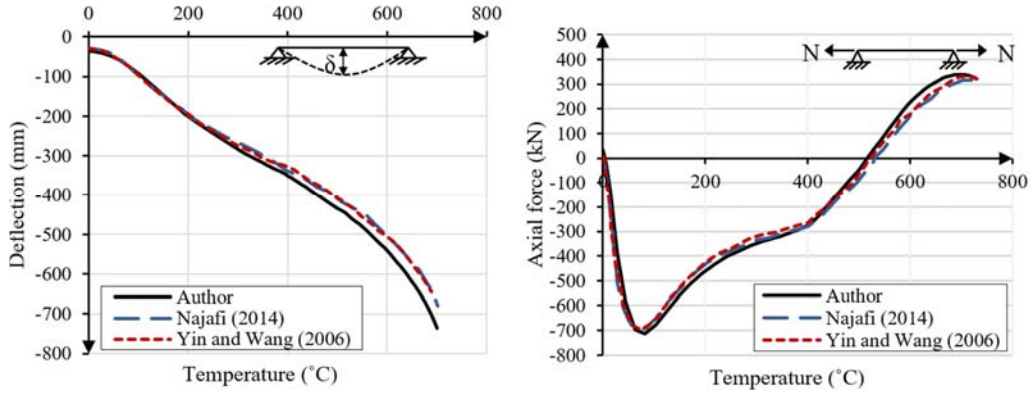

Fig. 10 Comparison of deflection-temperature (LHS) and axial force-temperature responses (RHS) from the simulation results of the author with those of Yin and Wang (2006) [23] and Najafi (2014) [24] for NOW

III. Parametric Study and Results

A. Details of Parametric Numerical Models

Having validated the FE models, parametric studies were conducted to study the behaviour of axially restrained beams at elevated temperature. For this reason, properties of both stainless steel (SS1.4571) and carbon steel (S275) were considered using multiple axial restraint stiffness ratio (α_A). Therefore, the difference between fire response of axially restrained stainless steel and carbon steel beams were compared under uniformly distributed load with load level of 30%, 50% and 70% of failure load for axially unrestrained beam at room temperature (Load ratios of LR:0.3, LR: 0.5 and LR:0.7). The lateral restraints were applied at every 500 mm span of the modelled beam to avoid lateral torsional buckling failure. The beam cross-section employed for all models in parametric study was IPE400 with height, width, web thickness and flange thickness equal to 400 mm, 180 mm, 8.6 mm, 13.5 mm respectively. The classification for the designated cross-section

Open Science Index, Civil and Architectural Engineering Vol:18, No:9, 2024 publications.waset.org/10013796.pdf

Open Science Index, Civil and Architectural Engineering Vol:18, No:9, 2024 publications.waset.org/10013796.pdf

was confirmed as Class 1 corresponding to the cross-section classification limits presented in EN 1993-1-4 [26]. The beam section was conventionally welded, and the beam length was 6000 mm for all models with the location of openings centre at mid-height of beam section. In reality, beams are not fully restrained due to the structural continuity in which different level of axial restraints (α_A) is provided by cooler columns or subframes to the end of heated beam. This approach was adapted in the numerical modelling. To evaluate the effect of axial restraint on the beam response in fire, the beam supports were assumed as i) pin-roller where $\alpha_A = 0$, ii) pin-pin which implies fully restraints and iii) multiple axial restraint stiffness ratios α_A equal to 0.02, 0.05, 0.15, 0.3, 0.5 and 1 while, rotational restraint was set to zero. The axial restraint stiffness ratio is defined as the ratio of the axial restraint stiffness to the axial stiffness of the beam at room temperature EA/L = 201.78 kN/mm, where E, A and L are respectively Young's modulus, area of cross-section and beam length. Since the rotational stiffness of connections in simple construction is low, the rotational restraints at beam end were not integrated in FE models. Also, the focus of this study is on catenary action in which the beam response is principally through axial tension and the contribution of beam flexure is negligible in beam large deflection.

The material properties for carbon steel plates were set for S275 and the room temperature material properties of austenitic stainless steel were adopted to the beam recommended by Afshan et al. [27] in the numerical parametric studies as reported in Table I. In the table , E is the Young's modulus, f_y is the yield stress taken as the 0.2% proof stress, f_u is the ultimate tensile stress, ε_u is the strain at the ultimate tensile stress and n and m are the two-stage Ramberg-Osgood model parameters. The reduction factors pertaining to grade EN 1.4571 provided in Table 8.1 of the Design Manual for Structural Stainless Steel [28] were employed. The two-stage Ramberg-Osgood model given by (3) and (4) was employed to construct full range stress-strain curves which were input into the FE models in the form of true stress and log-plastic strain.

TABLE I
MATERIAL PROPERTIES OF EN 1.4571 STAINLESS STEEL GRADE AT ROOM TEMPERATURE.

Stainless steel grade	E (N/mm^2)	f_y (N/mm^2)	f_u (N/mm^2)	ε_u	n	m
EN 1.4571	200000	280	580	0.5	9.1	2.3

$$\varepsilon_\theta = \frac{\sigma_\theta}{E_\theta} + 0.002\left(\frac{\sigma}{f_{y,\theta}}\right)^{n_\theta} \quad , \quad \sigma \le f_{y,\theta} \tag{3}$$

$$\varepsilon_\theta = \frac{\sigma_\theta - f_{y,\theta}}{E_{0.2,\theta}} + \varepsilon_{u,\theta}\left(\frac{\sigma_\theta - f_{y,\theta}}{f_{u,\theta} - f_{y,\theta}}\right)^{m_\theta} + \varepsilon_{y,\theta} \quad , \quad f_{y,\theta} < \sigma \le f_{u,\theta} \tag{4}$$

where σ_θ and ε_θ are respectively the stress and strain at temperature θ, $f_{y,\theta}$ is the yield stress, taken as the 0.2% proof stress, at temperature θ, E_θ is the Young's modulus at temperature θ, $E_{0.2,\theta}$ is the tangent modulus associated with $f_{y,\theta}$, $\varepsilon_{y,\theta}$ is the total strain corresponding to $f_{y,\theta}$, $\varepsilon_{u,\theta}$ is the strain at ultimate tensile stress $f_{u,\theta}$, and n_θ and m_θ are the Ramberg-Osgood model parameters at temperature θ.

The standard ISO 834 temperature-time curve given in EN 1992-1-2 [24] was used for the thermal model to apply the unfirm temperature distribution across the depth of cross-section. The convective heat transfer coefficient factor and the emissivity were taken as 25 W/(m^2 °C) and 0.4, respectively, as specified in EN 1993-1-2 [25]. Thermal properties including specific heat, thermal expansion and thermal conductivity as recommended in [28] for austenitic stainless steels were employed. The global imperfection amplitude was set to L/1000 for all stainless steel beams. The local imperfection amplitude ω_0 was taken as that predicted from the modified Dawson and Walker model adapted for stainless steel [29], given by (5), where t is the thickness, f_y is the material yield stress and $f_{cr,min}$ is the minimum elastic buckling stress of all the plate elements making up the cross-section.

$$\omega_0 = 0.023t\left(f_y / f_{cr,\min}\right) \tag{5}$$

The residual stress patterns associated with conventionally welded stainless steel I-sections were incorporated into the FE models. The magnitude and distribution of residual stresses in the conventionally welded stainless steel sections were studied experimentally by Yuan et al. [30], which was adopted in the numerical parametric models developed herein.

The key parameters to be evaluated in this section are: 1) eight different axial restraint levels of 0, 0.02, 0.05, 0.15, 0.3, 0.5, 1 and fully restraint to consider structural continuity in the analysis, 2) two opening shape including circle hole (CH) and elongated circle hole (EH) shapes, 2) three different ratios of opening height (d_0) to cross-section height (h) as d_0/h = 0.5, 0.65, and 0.75, 3) three load ratio (LR) of 0.3, 0.5, and 0.7, 4) two steel material categories including carbon steel (CS275) and stainless steel (SS1.4571), 5) five different number of web openings including 1, 3, 5, 6, and 9 web openings. The beams are labelled in the order of steel classification, opening depth d_0, number of openings, and shape of openings, e.g., SS1.4571 0.75h 9CH denotes stainless steel of grade 1.4571 with opening depth to cross-section height of 0.75 and 9 number of openings of a circle shape.

B. Effect of Structural Continuity on Axial Force and Deflection of Cellular Stainless Steel Beams

To evaluate the effect of load ratio on the performance of cellular beam subjected to elevated temperature, the results of mid-span deflection and axial force for fully restrained.

d beam with six number of elongated circles opening of d_0 = 0.65 h is presented in Fig. 12. It is shown that although the fire resistance of all beams is reduced by increasing the load ratio, the general beam response in fire, e.g., beam deflection and axial force is not affected by the load ratio. Overall, the results suggest that cellular beam performance is irrespective of the load ratios. Hence, to capture the influence of all restraints conditions as well as openings shape and size on the cellular

beam performance, all simulations shown in this section is presented for load ratio of 0.5.

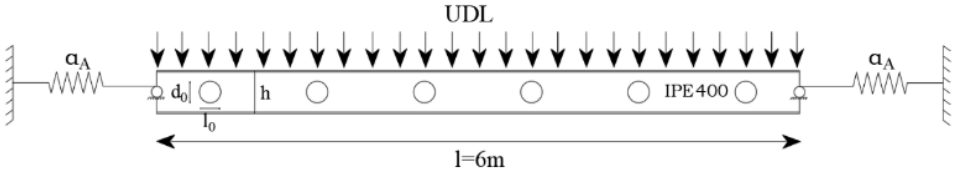

Fig. 11 Geometrical details of the beams with uniform temperature distribution for parametric study (0.5h 6CH)

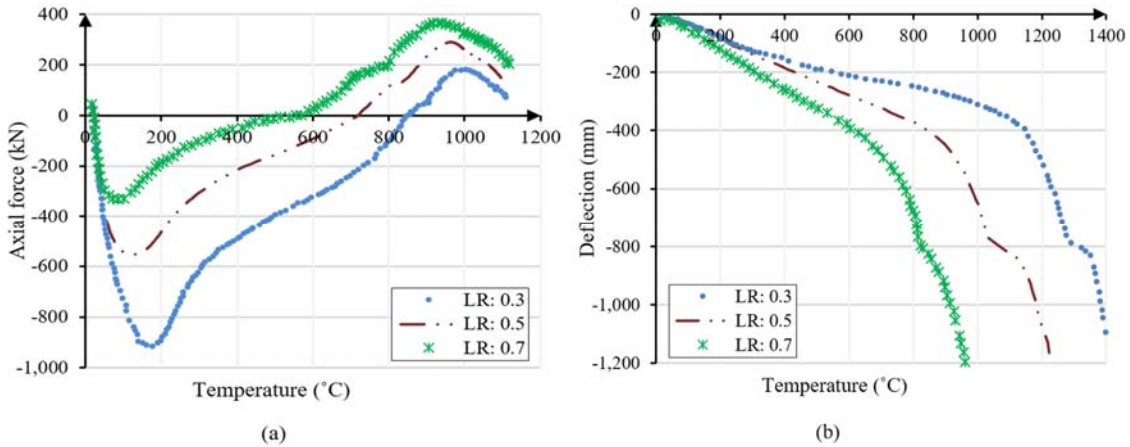

Fig. 12 The results of (a) axial force-temperature and (b) mid-span deflection-temperature for fully restrained stainless steel SS1.4571 cellular beam with 6 number of elongated circle openings and d0/h = 0.65 "SS1.4571 0.65h 6EH" under different load ratios

The results of axial force temperature for different load levels (Fig. 12 (a)) suggest opposite correlation between load level and temperature at the commence of catenary stage "beam transition temperature". The beam behaved similarly comparing axial force responses at elevated temperature regardless of the load level. The same behaviour was observed when deflection-temperature responses are investigated (Fig. 12 (b)). To have an overarching view of the behaviour of restrained cellular stainless steel beams, the figures are mainly chosen for six number of openings. The cellular beam with six numbers of openings showed slightly improved transit temperature at commencing catenary stage due to the configuration of openings and net distances between openings within the cross-section.

To evaluate the effect of structural continuity on fire response of cellular beam having circle and elongated circle shapes of opening, temperature at maximum tensile axial force of cellular beams with different web depth and shapes were presented in Fig. 13. According to Fig. 13, the temperature at maximum tensile axial force is reduced by increase in the axial restraint level for all cases. However, the reduction in temperature is much noticeable for small axial restraints ($\alpha_A < 0.15$). The temperature reduction became smoother for α_A above 0.15 and it was almost invisible for axial restraint greater than 0.4. This confirms that the temperature at which the cellular beam deflection starts to runaway is a function of the axial restraint stiffness and as can be seen in Fig. 13, is lower for beams with higher restraint stiffness. It is concluded that there is a critical axial restraint stiffness ratio beyond which there is no significant further reduction in failure temperature with increasing axial restraint stiffness. This critical level of axial restraint is found as 0.15 in this study. Comparing the temperature at maximum tensile axial force for different web opening size (d_0/h of 0.5, 0.65, 0.75) and different shape of opening in Fig. 13 displayed a great level of reliance of axially restrained cellular beam response on its opening shape and size. Most notably, it was concluded that the opening depth has the dominant influence amongst other parameters of web opening on cellular beam response at fire. The general performance of cellular beam was deteriorated by increasing the web opening height for all level of axial stiffness at beam connections. Following web height, the shape of web opening influences cellular beam performance in which the circular shape showed an improved response comparing with elongated circle shape.

It is seen that for high axial restraint i.e., α_A greater than 0.15, the transit temperature where the catenary stage was established, turned into the lowest temperature in its range. The difference between the temperature at the maximum tensile force within the beam cross section (θ_f) and the transit temperature (θ_{tr}) is a quite significant value, where the temperature difference is denoted by $\Delta\theta$. This confirms unrealistic approach of setting transit temperature at the heart of beam design in fire and ensuring the beam end connection safety. To guarantee connection safety, it is required to find the maximum tension force within the beam cross-section. The maximum tensile axial force in catenary stage was increasing

Open Science Index, Civil and Architectural Engineering Vol:18, No:9, 2024 publications.waset.org/10013796.pdf

Open Science Index, Civil and Architectural Engineering Vol:18, No:9, 2024 publications.waset.org/10013796.pdf

with the level of axial restraint due to the higher axial restraint in combination with temperature expansion of the beam. Comparing the shape of web opening, the beam with circle web openings showed a higher transit and failure temperature for the same opening height. It is essential to make sure that the catenary tension force for temperature beyond transit temperature can be resisted by the connection until the maximum tensile force is reached at failure temperature. Increasing the depth of opening was shown to drastically decrease the transit temperature. This was opposite to the change in $\Delta\theta$ by increasing the opening depth. The effectiveness of computing $\Delta\theta$ is to predict the transit temperature of the axially restrained beam to evaluate the large deflection development. The analytical equation to calculate $\Delta\theta$ was suggested for steel cellular beam [24] based on examination of the numerical results which was prominently influenced by the slenderness of the top tee-section λ_t and the level of axial restraints. This is the foundation for the future work of this study on developing a design method for stainless steel cellular beams in fire.

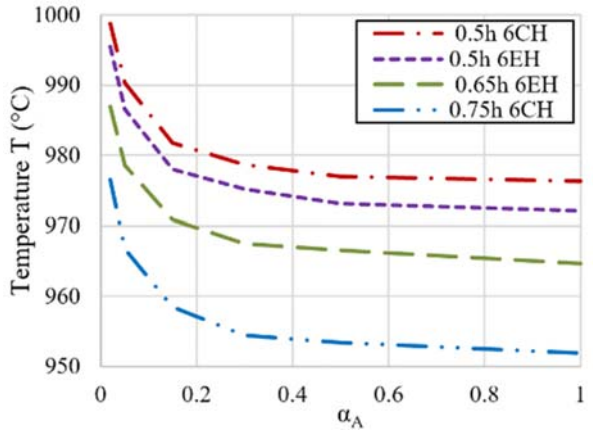

Fig. 13 Temperature at maximum tensile force against axial restraint level for opening shape and depth

According to Fig. 13, the drop in the transit temperature was quantified as about 10% as the average rate over the full range of restraint ratios once the depth of circle web opening is changed from 0.5 h to 0.75 h. The rise of transit temperature for elongated circle web when the depth was expanded from 0.5 h to 0.65h, was limited to about 2.3%. The reason for this behaviour is that increase in the opening depth of the beam reduces the internal shear and moment resistance of the beam which leads to decrease in the shear and flexural failures. In case of elongated circle opening shape, while the local shear and moment resistance are not influenced by the opening length, the local Vierendeel moment is directly proportional to the opening length. In total, any increase in the size of web opening in particular for the depth above half of the web height, will lower the resistance of the beam to the shear, moment and Vierendeel moment. The general performance of cellular stainless steel beam with six small openings when the depth was limited to 0.5 h and for length of opening between d_0 and $2d_0$, was similar to the beam without opening as the of tee-sections at the top and bottom of web opening are less prone to buckle. Moreover, the increase pattern of mid-span deflection while axial forces turn from compression to tension was steady. The axial force-temperature for the stainless steel beams with circle and elongated circle web opening shapes under full range of restrained ratios is given in Figs. 14 (a)-(d) considering depth of web opening as 0.5, 0.65 and 0.75 of cross-section height.

In Fig. 14, it is observed that with increasing temperature, the compressive axial force, induced by restrained thermal expansion, becomes more pronounced, especially under higher axial restraint level. This force reaches a peak, beyond which significant deflection occurs, leading to large deformations as the axial force diminishes. The study also reveals that when a large opening is located at the centre of the beam—where tensile axial forces are maximal—the cellular stainless steel beam exhibits tensile behaviour at a comparatively lower temperature. It is shown that for large opening depth placed at the beam centre where the tensile axial force is at its maximum, the cellular stainless steel beam undergoes tensile action at a lower temperature. The reason is for superiority of axial buckling resistance of the slender tee-sections resulting in early buckling of the opening region. The transit temperature for small opening when d_0 = 0.5 h for both circle and elongated circle opening shape is respectively about 750 °C and 730 °C for all axial restraint level establishing superior behaviour for circle shape of openings. Comparing axial reaction forces for all level of restraints, it is observed that the transit temperature is approximately independent of the axial restraints' ratios for stainless steel cellular beam with small opening size. This behaviour can be explained by the fact that in tee-sections with small openings, where buckling is not a factor, the moment generated by axial forces corresponds to the diminished moment capacity of the opening at the transition temperature. However, for larger openings, where the unloading of the tee-sections after initial failure causes immediate entering into catenary action, the post-buckling behaviour of tee-sections governs the behaviour of cellular beams. The transit temperature of stainless steel cellular beam when the depth of opening was expanded from 0.5 to 0.65 and 0.75 of web height remained constant once the axial restrained ratio was above 0.15. For the beam with axial restraint ratios lower than 0.15, the transit temperature was slightly higher. Comparing temperature at the maximum tensile axial force in catenary stage for all cases, beams with circle shape of web opening and d_0 = 0.5 h demonstrated the highest temperature (975 °C) and improved fire performance. At the highest tensile force, the bottom tee-section reaches the maximum axial tension in which the axial force is equal to the maximum tensile capacity of the beam with zero axial force in the top tee-sections causing a failure to the connections. The minimum temperature for reaching the maximum tensile force is captured for the beam with opening depth of d_0 = 0.75 h and web opening shape of elongated circle. This indicates that the magnitude of the axial tensile force generated during the catenary action stage substantially depends on the size, and shape of the web openings. This part of the study demonstrated a direct proportionality between the tensile force in the catenary stage

and the degree of axial stiffness. Specifically, cellular beams subjected to lower axial restraints exhibited reduced tensile forces at elevated temperatures. This led to an increased failure capacity at the connections, particularly when the axial restraint level was below 0.15. It was seen that in general, the circular opening performs best compared to the elongated circle shape of opening for same opening depth. Also, the results from this section show that the response of cellular beams was affected prominently by the height of opening comparing to the effect of opening shape.

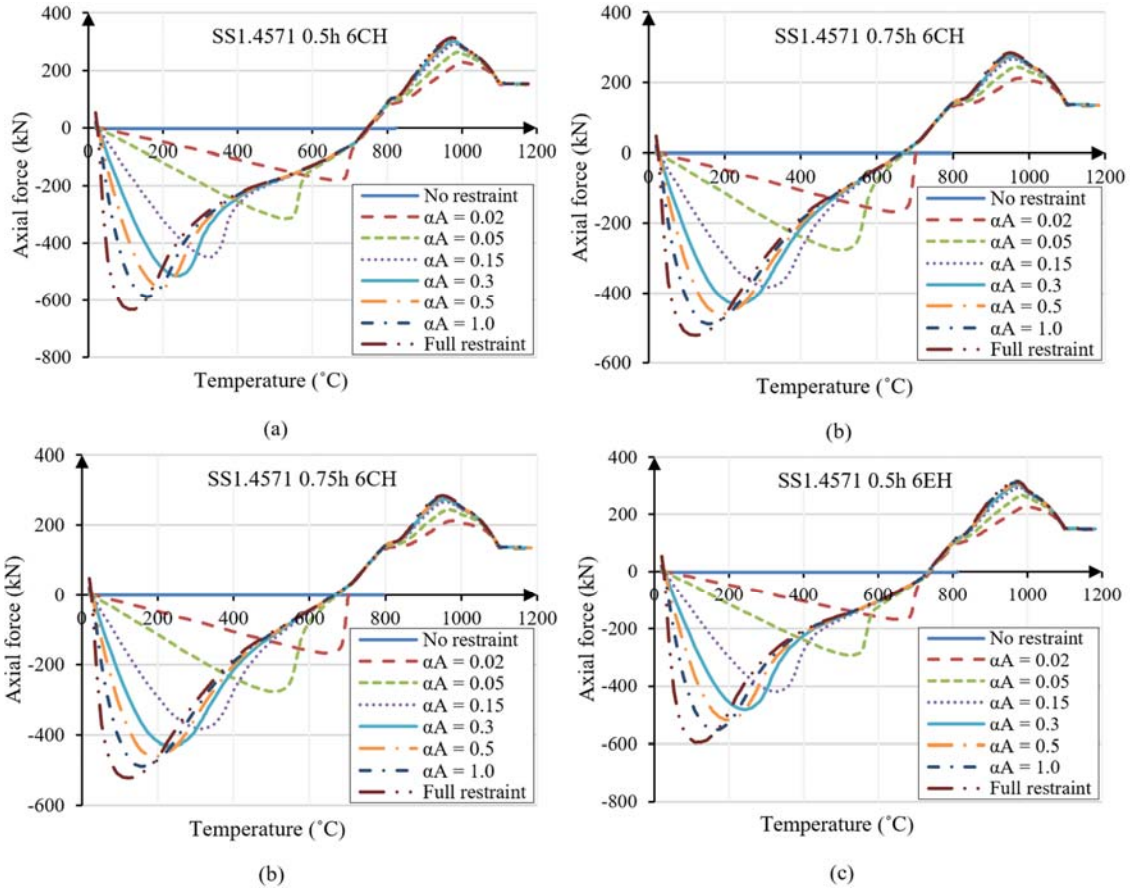

Fig. 14 Results of axial force-temperature for stainless steel (SS1.4571) cellular beam with 6 number of web openings for (a) circle opening shape and d0/h = 0.5, (b) circle opening shape and d0/h = 0.75, (c) elongated circle web opening and d0/h = 0.5, and (d) elongated circle web opening and d0/h = 0.65

C. Comparison of Stainless Steel and Carbon Steel Cellular Beam

The substantial effect of structural continuity with the application of different level of axial restraints on the performance of carbon steel and stainless steel cellular beams is shown in Figs. 15 and 16 where the cellular beams with nine large circular web openings of $d_0 = 0.75$ h were investigated to evaluate the weakest section amongst all considered cases. Given that the beam length is 6000 mm, the presence of nine large openings results in a weakened section, attributable to the reduced net spacing between the openings. It was observed that carbon steel cellular beam performance extremely depends on the level of axial restraints. The transit temperature of cellular carbon steel beam was decreased 111 °C when the axial restraints increase from 0.02 to fully restrained condition. The same behaviour was captured in case of assessing the deflection of carbon steel beam with large openings. However, as can be seen in Fig. 16 (a), the transit temperature for stainless steel was merging when axial restraint is above 0.15.

Figs. 17 and 18 compare respectively the axial reaction force-temperature and deflection-temperature for the axially restrained stainless steel and carbon steel cellular beams with circle web opening and $d_0 = 0.5$ h covering full range of axial restraint ratios. As can be seen, due to the higher level of compressive axial force, the stainless steel cellular beam deflects higher than carbon steel cellular beams preceding to the inception of large deflections. This behaviour results from higher thermal expansion of stainless steel beams. The transit temperature of stainless steel cellular beam is the same for all level of axial restraint stiffness particularly when $\alpha_A > 0.15$. However, the transit temperature of carbon steel cellular beam is in general reduced by increasing the level of axial restraints. The large deflection for stainless steel cellular beams starts at higher temperature due to the superior material properties and strength of stainless steel beams. Overall, the stainless steel cellular beams show higher tensile forces at significantly higher temperature (978 °C) in the catenary stage that may cause a failure to the connection at much higher temperature in

Open Science Index, Civil and Architectural Engineering Vol:18, No:9, 2024 publications.waset.org/10013796.pdf

comparison with carbon steel cellular beam (723 °C).

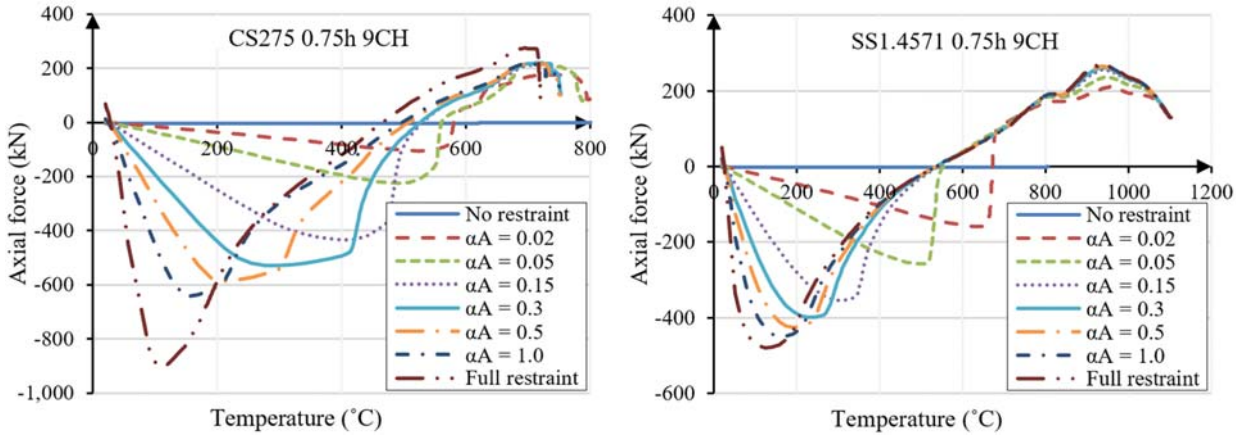

(a) (b)

Fig. 15 Results of axial force-temperature relationship for carbon steel CS275 (a) and stainless steel SS1.4571; (b) cellular beams, each with nine openings and a d0/h ratio of 0.75, across all axial restraint ratios

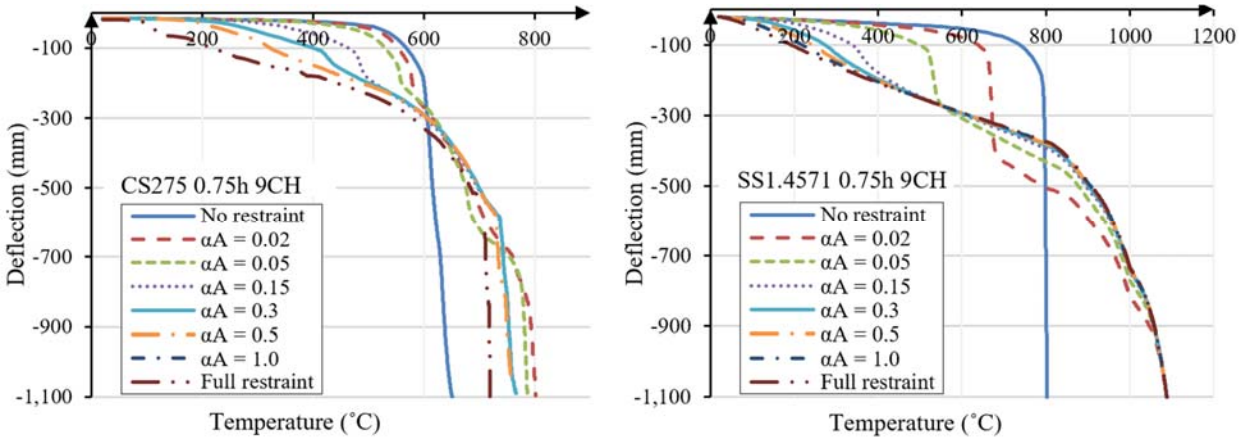

(a) (b)

Fig. 16 Results of mid-span deflection-temperature for carbon steel CS275 (a) and stainless steel SS1.4571; (b) cellular beam with nine number of openings and d0/h = 0.75 over the full range of axial restraint ratios

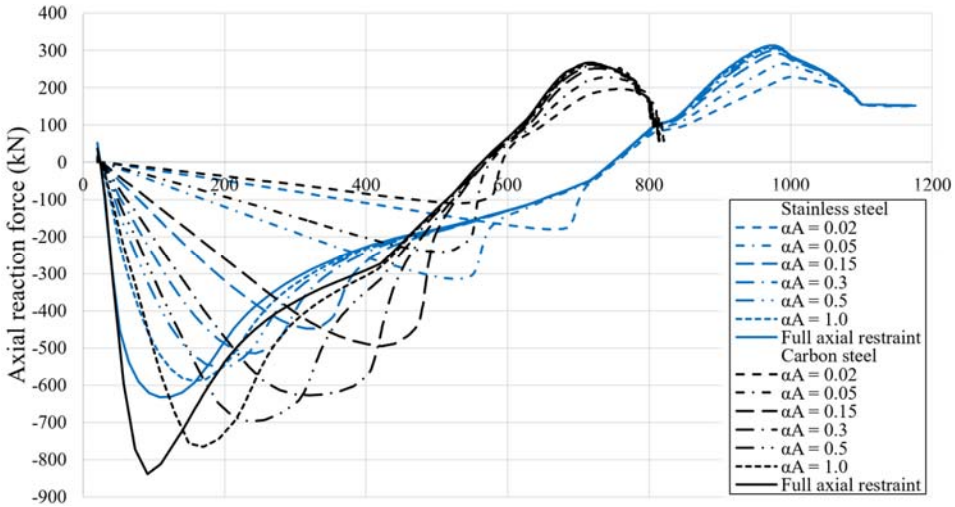

Fig. 17 Comparison of axial force-temperature responses of axially restrained stainless steel and carbon steel beams for 6 number of web opening with d0/h = 0.5

Open Science Index, Civil and Architectural Engineering Vol:18, No:9, 2024 publications.waset.org/10013796.pdf

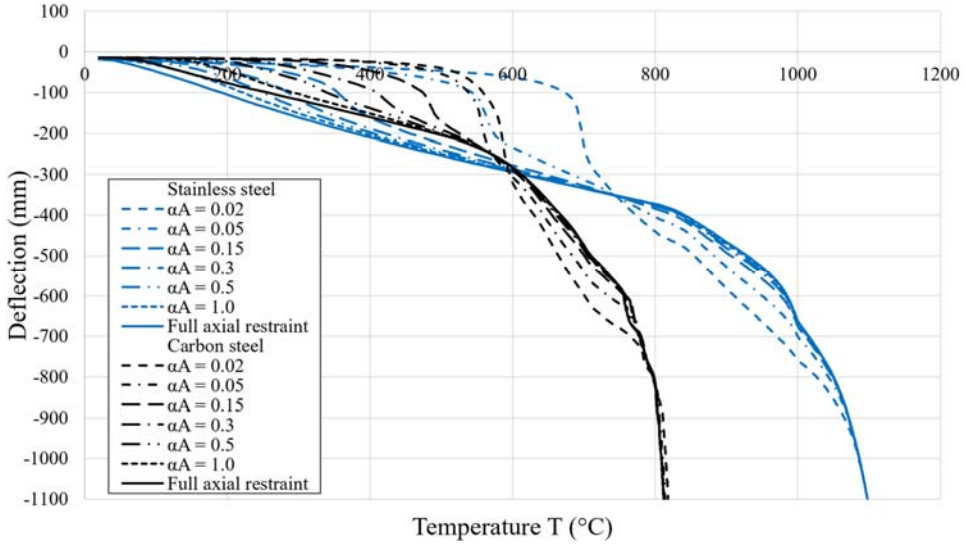

Fig. 18 Comparison of deflection-temperature responses of axially restrained stainless steel and carbon steel beams for 6 number of opening with d0/h = 0.5

Investigating deflection-temperature of stainless steel and carbon steel cellular beam in Fig. 18, a noticeable large deflection for temperature above 600 °C and 800 °C is shown for carbon steel and stainless steel respectively. Since the beam is still survived by developing axial tensile force in tee-section beyond transition temperature to temperature about 740 °C and 980 °C for carbon steel and stainless steel respectively, the large deflection for axially restrained beams cannot be interpreted as impending run-away failure. These large deflections are induced by restrained thermal expansion which are not a sign of capacity loss for the cellular beam at elevated temperatures. This behaviour of restrained cellular beams shows how replacing bending by catenary action delays run-away deflection of beam at fire by causing the beam to act as a cable in pure tension hanging at the connections to the adjacent structures.

Figs. 17 and 18 illustrate that axially restrained stainless steel cellular beam experiences similar stages of behaviour in fire that the carbon steel cellular beam developed. However, higher transit temperature for commencing catenary stage and failure temperature of cross-section were observed for stainless steel cellular beam. The stainless steel cellular beam shows an average of respectively 24% and 26% higher transit temperature and temperature at the maximum tensile axial force than carbon steel. This reveals that despite the higher thermal expansion for stainless steel cellular beam, it is capable of withstanding higher temperature before onset of large deflection and commencing catenary stage. The improved fire response of stainless steel is due to the accompanying favourable strength and stiffness retention factors at high temperature for stainless steel beams. It is also worth it to note that the transit temperature of stainless steel is not extensively affected by changing axial restraint ratio particularly when $\alpha_A >$ 0.15, however, transit temperature of carbon steel is decreasing when the connections induce stronger axial restraints.

IV. Conclusion

To assess the response of large deflection behaviour of axially restrained stainless steel cellular beams in fire, a numerical modelling study was conducted. At the first step, the simulations of carbon steel cellular beam with different rectangular web opening exposed to fire from two sources of literature were replicated using finite element analysis package ABAQUS to produce a validated numerical modelling procedure. Following validating the results from literature, a parametric study was carried out with the main focus on the effect of axial restraints level on fire response of carbon steel and stainless steel cellular beams. It was shown that while the general response of carbon steel and stainless steel cellular beam with various level of axial restraints in fire is similar, the transit temperature of stainless steel cellular beams are less affected by stiffness of axial restraints. The stainless steel cellular beam deflected more than carbon steel ones for higher axial restraints due to higher thermal expansion when $\alpha_A > 0.15$. The critical level of axial restraint in which the temperature at the onset of catenary action and at the location of maximum tensile force become independent from level of restraints, was found as 0.15 for stainless steel cellular beams in fire. At the transition temperature of stainless steel cellular beams, there is a direct proportionality between the maximum axial tensile force and the degree of axial restraint. Furthermore, according to the results of this study, the response of cellular beam for any axial restraint is significantly dependent on respectively the depth of web openings and shape of web openings. Future work will focus on the development of a design method for stainless steel cellular beams in fire taking into consideration the influences of axial restraint stiffness on the cellular beam failure mode and the failure temperature.

Acknowledgment

This research was supported by the University of Hertfordshire which is gratefully acknowledged.

Open Science Index, Civil and Architectural Engineering Vol:18, No:9, 2024 publications.waset.org/10013796.pdf

Open Science Index, Civil and Architectural Engineering Vol:18, No:9, 2024 publications.waset.org/10013796.pdf

REFERENCES

[1] R. M. Lawson, and S. J, Hicks, "Design of Composite Beams with Large Web Openings", *Steel Construction Institute (SCI)*, Ascot, 2011.

[2] F. Erdal, "Ultimate Load Capacity of Optimally Designed Cellular Beams", PhD Thesis, Middle East Technical University, Turkey, 2011

[3] L. F. Grilo, R. H. Fakury, A. L. de Castro e Silva, and G. de Souza Verissimo, "Design procedure for the web-post buckling of steel cellular beams", *Journal of Constructional Steel Research*, vol. 148, 2018, pp. 525-541.

[4] K. F. Chung, T. C. H. Liu, and A. C. H. Ko, "Investigation on Vierendeel mechanism in steel beams with circular web openings", *Journal of Constructional Steel Research*, vol. 57, 2001, pp. 467-490.

[5] K. D. Tsavdaridis, and C. D. Mello, "Web buckling study of the behaviour and strength of perforated steel beams with different novel web opening shapes", *Journal of Constructional Steel Research*, vol. 67, no. 10, 2011, pp. 1605-1620.

[6] L. Kang, S. Hong, and X. Liu, "Shear behaviour and strength design of cellular beams with circular or elongated openings", *Thin-walled Structures*, vol. 160. no. 4, 2021, Article 107353.

[7] V. Y. B. Wong, I. W. Burgess, and R. J. Plank, "Behavior of composite floor beam with web openings at high temperatures", *in SDSS'Rio 2010 Stability and Ductility of Steel Structures*, P.V. E. Batista, L. de Lima (Eds.), Editor, Rio de Janeiro, Brazil, 2010.

[8] L. Wang, J. Li, C. Luo, X. Cao and H. Wang, "Experimental and numerical study on the shear behaviour of web perforated cold-formed steel beams", *Structures*, vol. 45, 2022, pp. 2117-2136.

[9] F. De'nan, N. S. Hashim, and L. K. Zenth, "Finite element analysis of perforated cold-formed steel section: Effects of shear behavior", *Journal of structural monitoring and built environment*, vol. 1, no. 1, 2021, pp. 18-27.

[10] P. Sangeetha, S. M. Revathi, V. Sudhakar, D. Swarnavarshini, and S. Sweatha, "Behaviour of cold-formed steel hollow beam with perforation under flexural loading", *Materials Today: Proceedings*, vol. 38, 2021, pp. 3103-3109.

[11] N. R. Baddoo, "100 years of stainless steel: A review of structural applications and the development of design rules", *The Structural Engineer*, vol. 91, no. 8, 2013, pp. 10-18.

[12] S. G. Morkhade, and L. M. Gupta, "Experimental investigation for failure analysis of steel beams with web openings", *Steel and Composite Structures*, vol. 23, 2017, pp. 647-656.

[13] F. Rodrigues, P. C. G. Vellasco, L. R. O. Lima, and S. A. L. Andrade, "Finite element modelling of steel beams with web opening", *Engineering*, vol. 6, 2014, pp. 886-913.

[14] T. C. H. Liu, and K. F. Chung, "Steel beams with large web openings of various shapes and sizes: finite element investigation", *Journal of Constructional Steel Research,* vol. 59, 2003, pp. 1159-1176.

[15] K. T. Ng, "Stainless steel structures in fire", PhD thesis, 2007.

[16] A. Nadjai, C. G. Bailey, O. Vassart, S. Han, W. I. Simms, M. Hawes, B. Zhao, and J. M. Franssen, "Full -scale fire test on a composite floor slab incorporating long span cellular steel beams", *Journal of The Structural Engineer*, vol. 89, 2011, pp. 18-25.

[17] K. A. Cashell, M. Malaska, M. Khan, M. Alanen, and K. Mela, "Experimental and numerical analysis of stainless steel cellular beams in fire", *Fire Safety Journal*, vol. 121, 2021, pp. 103277-103277.

[18] A. Pournaghshband, S. Afshan, and M. Theofanous, "Elevated temperature performance of restrained stainless steel beams", *Structures*, vol. 22, 2019, pp. 278-290.

[19] A. M. Allam, I. W. Burgess, and R. U. Plank, "Performance-based simplified model for a steel beam at large deflection in fire", *Proc. of the 4th Int. Conf. on Performance-based Codes and Fire Safety Design Methods*, Melbourne, Australia, 2002.

[20] Y. Z. Yin, and Y. C. Wang, "Analysis of catenary action in steel beams using a simplified hand calculation method, Part 1: theory and validation for uniform temperature distribution", *Journal of Constructional Steel Research*, vol. 61, 2004, pp. 183-211.

[21] L. Chen, and Y. C. Wang, "Methods of improving survivability of steel beam/column connections in fire", *Journal of Constructional Steel Research*, vol. 79, 2012, pp. 127-139.

[22] ABAQUS/CAE Standard User's Manual, version 2023. Dassault Systèmes Simulia Corp.

[23] Y. Z. Yin, and Y. C. Wang, "Analysis of behaviour of steel beams with web openings at elevated temperatures", *Steel and Composite Structures,* vol. 6, 2006, pp. 15-31.

[24] M. Najafi, "Behaviour of axially restrained steel beams with web openings at elevated temperature", PhD thesis, 2014.

[25] EN 1993-1-2, Eurocode 3: Design of steel structures - Part 1.2: General rules – Structural fire design, Brussels: European Committee for Standardization (CEN), 2005.

[26] EN 1993-1-4, Eurocode 3: Design of Steel Structures – Part 1.4: General Rules – Supplementary Rules for Stainless Steels, European Committee for Standardization (CEN), Brussels, 2015.

[27] S. Afshan, O. Zhao, and L. Gardner, "Standardised material properties for numerical parametric studies of stainless steel structures and buckling curves for tubular columns", *Journal of Constructional Steel Research*, vol. 152, 2018, pp. 2-11.

[28] Design Manual for Structural Stainless Steel, Forth Edition, Steel Construction Institute, 2017.

[29] R. G. Dawson, and A. C. Walker, "Post-buckling of geometrically imperfect plates", *Journal of the Structural Division (ASCE)*, vol. 98, no. 1, 1972, pp. 75-94.

[30] H. X. Yuan, Y. Q. Wang, Y. J. Shi, and L. Gardner, "Residual stress distributions in welded stainless steel sections", *Thin-Walled Structures*, vol. 79, 2014, pp. 38–51.